

<sup>1</sup> **High-resolution regional climate model evaluation using variable-resolution**

<sup>2</sup> **CESM over California**

<sup>3</sup> Xingying Huang, \* Alan M. Rhoades and Paul A. Ullrich

<sup>4</sup> *Department of Land, Air and Water Resources, University of California, Davis*

<sup>5</sup> Colin M. Zarzycki

<sup>6</sup> *National Center for Atmospheric Research*

<sup>7</sup> \*Corresponding author address: Xingying Huang, Department of Land, Air and Water Resources,

<sup>8</sup> University of California Davis, Davis, CA 95616.

<sup>9</sup> E-mail: xyhuang@ucdavis.edu

## ABSTRACT

10 Understanding the effect of climate change at regional scales remains a topic  
11 of intensive research. Computational constraints have meant that the high hor-  
12 izontal resolutions required to reach regional scales have been largely out of  
13 reach of modern global climate models. However, high horizontal resolution  
14 is needed to represent topographic forcing, which is a significant driver of  
15 local climate variability. Although regional climate models (RCMs) have tra-  
16 ditionally been used at these scales, variable-resolution global climate mod-  
17 els (VRGCMs) have recently arisen as an alternative for studying regional  
18 weather and climate. In this paper, the recently developed variable-resolution  
19 option within the Community Earth System Model (CESM) is assessed for  
20 long-term regional climate modeling. The mean climatology across Califor-  
21 nia's diverse climate zones, including temperature and precipitation, is ana-  
22 lyzed and contrasted with the Weather Research and Forcasting (WRF) model  
23 (as a traditional RCM), regional reanalysis, gridded observational datasets and  
24 uniform high-resolution CESM with the finite volume (FV) dynamical core.  
25 The results show that variable-resolution CESM is competitive in representing  
26 regional climatology on both annual and seasonal time scales. This assess-  
27 ment adds value to the use of VRGCMs for projecting climate change over  
28 the coming century and improve our understanding of both past and future  
29 regional climate related to fine-scale processes. This assessment is also rele-  
30 vant for addressing the scale limitation of current RCMs or VRGCMs when  
31 next-generation model resolution increases to  $\sim$ 10km and beyond.

<sup>32</sup> **1. Introduction**

<sup>33</sup> Global climate models (GCMs) have been widely used to simulate both past and future cli-  
<sup>34</sup> mate. Although GCMs have demonstrated the capability to successfully represent large-scale  
<sup>35</sup> features of the climate system, they are usually employed at coarse resolutions ( $\sim 1^\circ$ ), largely  
<sup>36</sup> due to computational limitations. Global climate reanalysis datasets, which assimilate climate  
<sup>37</sup> observations using a global model, represent a best estimate of historical weather patterns, but  
<sup>38</sup> still have relatively low resolutions no finer than  $0.5^\circ$  (<http://reanalyses.org/atmosphere/>  
<sup>39</sup>) overview-current-reanalyses). Consequently, regional climate is not well captured by either  
<sup>40</sup> GCMs or global reanalysis datasets. However, dynamical processes at unrepresented scales are  
<sup>41</sup> significant drivers for regional and local climate variability, especially over complex terrain (?).

<sup>42</sup> In order to capture these fine-scale dynamical features, high horizontal resolution is needed to al-  
<sup>43</sup> low for a more accurate representation of fine-scale forcings, processes and interactions (??). We  
<sup>44</sup> anticipate that with these enhancements the regional climate information will be more usable for  
<sup>45</sup> policy makers and local stakeholders in formulating climate adaptation and mitigation strategies.

<sup>46</sup> In order to model regional climate at high spatial and temporal resolution over a limited area,  
<sup>47</sup> downscaling methods have been developed. There are largely two approaches for downscaling:  
<sup>48</sup> The first is statistical downscaling, which aims to estimate fine scale behavior via analysis of the  
<sup>49</sup> statistical relationships between observed small-scale variables and larger (GCM) scale variables  
<sup>50</sup> (?). This method is empirical and cannot be used if the observed relationships do not hold with  
<sup>51</sup> a changing climate (?). The second approach is dynamical downscaling, which uses a numerical  
<sup>52</sup> model to simulate higher spatial resolution conditions in greater detail. Dynamical downscaling is  
<sup>53</sup> popular and commonly employed using nested limited-area models (LAMs) or **by using a variable**  
<sup>54</sup> **resolution GCM (VRGCM) to model regional scales** (?). In this context, LAMs are typically

55 referred as regional climate models (RCMs) when applied to climate scales. RCMs are forced by  
56 output of GCMs or reanalysis data, and have been widely used, particularly to capture physically  
57 consistent regional and local circulations at the needed spatial and temporal scales (???). Recently,  
58 VRGCMs have been increasingly employed for modeling regional climate. This approach uses a  
59 global model that includes high-resolution over a specific region and lower resolution over the  
60 remainder of the globe (??). **Within VRGCM, there are also different strategies of achieving**  
61 **high-resolution over the area of interest such as stretched-grid models or grid refinement (??)..**  
62 VRGCMs have been demonstrated to be effective for regional climate studies and applications,  
63 owing to the advantages of traditional GCMs in representing large-scale features, at a reduced  
64 computational cost compared to uniform GCMs (??????).

65 Compared with RCMs, a key advantage of VRGCMs is that they use a single, unified modeling  
66 framework, rather than a separate GCM and RCM. Thus, VRGCMs avoid potential inconsistency  
67 between the global and regional domains, and naturally support two-way interaction between these  
68 domains without the need for nudging (????). However, in order to obtain deeper insight into the  
69 performance of these two modeling approaches, it is necessary to compare them directly. For the  
70 purposes of this paper, we will focus on the recently developed variable-resolution Community  
71 Earth System Model (varres-CESM) using as grid refinement technique as our VRGCM of in-  
72 terest. Although CESM has been well-used for uniform resolution modeling, variable-resolution  
73 in the Community Atmosphere Models (CAM) Spectral Element (SE) dynamical core has only  
74 been recently developed and has yet to be rigorously investigated for long-term regional climate  
75 simulation (??). Consequently, the goal of this paper is to evaluate the performance of varres-  
76 CESM against gridded observational data, reanalysis data and in comparison to a RCM. **Also,**  
77 **outputs from a uniform high-resolution CESM simulation have been utilized here ?.** Our variable-  
78 resolution simulations will focus on relatively high resolutions for climate assessment, namely

79 28km and 14km regional resolution, which are much more typical for dynamically downscaled  
80 studies. For comparison with the more widely used RCM method, the Weather Research and  
81 Forecasting (WRF) model will be used (?). We anticipate that this assessment will add value in  
82 modeling mean regional climatology and improve our understanding about the effects of multi-  
83 scale processes in regional climate regulation. Our goal is also to advance the understanding of  
84 better use of models in future climate predictions and climatic extremes studies regionally.

85 With its complex topography, coastal influences, and wide latitudinal range, this makes CA  
86 an excellent test bed for high-resolution climate studies. Also, an understanding of local cli-  
87 mate variability is incredibly important for policymakers and stakeholders in California due to its  
88 vast agricultural industry, wide demographics, and vulnerability to anthropogenically-induced cli-  
89 mate change (??). RCM simulations over California have also been conducted in previous studies  
90 (?????). ?, in particular, presented results from WRF (Weather Research and Forecasting) at 12km  
91 spatial resolution showing both the overall consistency and some biases between simulations and  
92 observations. **more details are to be added?**

93 This paper is organized as follows. Section 2 describes the model setup, evaluation methods  
94 and verification data. In section 3, results are demonstrated focusing on 2 m temperature (Ts) and  
95 precipitation (Pr). Key results are summarized along with further discussion in section 4.

## 96 **2. Models and Methodology**

### 97 *a. Simulation design*

98 All simulations use the AMIP (Atmospheric Model Intercomparison Project) protocols (?).  
99 AMIP simulations attempt to recreate a climatology similar to that observed over the past few

100 decades. The ocean model is disabled and the model is forced with prescribed sea-surface temper-  
101 atures (SSTs) and ice concentrations.

102 1) VARRES-CESM

103 CESM is a state-of-the-art Earth modeling framework developed by the National Center for At-  
104 mospheric Research (NCAR), consisting of atmospheric, oceanic, land and sea ice components  
105 and has been heavily used for understanding the effects of global climate change (??). **Differ-**  
106 **ent component models are connected by a couple component. In this way, the interfacial states**  
107 **and fluxes between the various component models are communicated and the fluxed quantities**  
108 **are conserved. Since we follow AMIP protocols in this study, communication is mainly occurred**  
109 **between atmospheric and land model. Ocean model and sea ice component are disabled.** Here,  
110 CAM version 5 (CAM5) (?) and the Community Land Model (CLM) version 4 (?) are used. As  
111 mentioned earlier, SE was used as the dynamical core in CAM along with the variable-resolution  
112 grid support. The FAMIP5 (F\_AMIP\_CAM5) compset was chosen for the simulations as it is the  
113 standard protocol for AMIP and is less computationally demanding. For our study, the variable-  
114 resolution cubed-sphere grids are generated for use in CAM and CLM with the open-source soft-  
115 ware package SQuadGen (?). The grids used are depicted in Figure 2. The maximum horizontal  
116 resolution on these grids are 0.25 degree ( $\sim 28\text{km}$ ) and 0.125 degree ( $\sim 14\text{km}$ ), with a 1 degree  
117 resolution covering the rest of the globe. These resolutions have been selected because CAM-SE  
118 naturally supports a 2:1 aspect ratio, meaning there are two transition layers from 1 degree to  
119 0.25 degree, and one additional transition from 0.25 degree to 0.125 degree. The time period is  
120 from 1979-01-01 to 2005-12-31 (UTC), and year 1979 was discarded as spin up time for CLM4.0.  
121 Variable-resolution topography files have been produced by starting with the **National Geophysical**  
122 **Data Center (NGDC) 2-min ( $\sim 3.5\text{ km}$ ) Gridded Global Relief Dataset (ETOPO2v2) topography**

123 dataset and applying the differential smoothing technique by adjusting the c parameter from Eq.  
124 (1) in ? add more details?. Land surface datasets, and plant functional types, were created at the  
125 standard 0.50 degree resolution. Greenhouse gas (GHG) concentrations are prescribed based on  
126 historical observations. SSTs and ice coverage are supplied by the 1degree Hadley Centre Sea Ice  
127 and Sea Surface Temperature dataset (HadISST) (?). Tuning parameters are not modified from  
128 their default configuration.

## 129 2) UNIFORM CESM

130 Output from a globally uniform CESM run at 0.25° global spatial resolution is utilized for com-  
131 parison. This globally uniform simulation uses the CAM5-FV (finite volume) dynamical core and  
132 is described in additional detail in ? and ?. Note that the appendix of the latter paper lists param-  
133 eters that are different from the public release. need to add details about this and which parameters  
134 are different from the public version.

## 135 3) WRF

136 WRF has gained wide acceptance in studying regional climate over the past decade, showing its  
137 adequate capability in representation of fine-scale climate properties (???). In this study, the fully  
138 compressible non-hydrostatic WRF model in version 3.5.1 with the Advanced Research WRF  
139 (ARW) dynamical solver is used. ERA (ECMWF re-analysis)-Interim surface and pressure-level  
140 reanalysis was used to provide initial and lateral conditions for the domains. The lateral conditions  
141 and SSTs were updated every 6 hours. ERA-Interim reanalysis (~80 km) has been widely used  
142 and validated for its reliability as forcing data (?). Two simulations are conducted with horizon-  
143 tal resolution of 27km and 9km simultaneously, over the time period 1979-01-01 to 2005-12-31

<sup>144</sup> (UTC). The year 1979 is used as a spin-up period and is discarded for purposes of analysis. The  
<sup>145</sup>  $\sim 10$  km resolution is actually finer than most previous studies for long-term climate.

<sup>146</sup> The simulation domains of WRF 9km are depicted in Figure 1. For the WRF 27km simulation,  
<sup>147</sup> one domain is used. For the WRF 9km simulation, two nested domains are used with the outer  
<sup>148</sup> domain at 27km (same as the WRF 27km) and inner domain at 9km horizontal grid resolution.

<sup>149</sup> **As a common way in WRF, two-way nesting is enabled by feeding back information from the fine  
150 grid onto the coarse grid, thus the nested region's process of the coarse domain is replaced by the  
151 fine grid result (?)**. These choices have been made to satisfy the natural WRF refinement ratio of

<sup>152</sup> 3:1. Both grids are centered on CA and have respectively,  $120 \times 110$  and  $151 \times 172$  grid points.

<sup>153</sup> Around the boundaries, 10 grid points are used as lateral relaxation zones. In order to reduce the  
<sup>154</sup> drift between forcing data and RCM, grid nudging (?) was applied to the outer domain every 6

<sup>155</sup> hours at all levels except the planetary boundary layer (PBL) as suggested by ?. This setup uses  
<sup>156</sup> 41 vertical levels with model top pressure at 50 hPa. **The topography data used in 27km and 9km  
157 are interpolated from USGS (U.S. Geological Survey) elevation data with 10m and 2m resolution  
158 respectively.**

<sup>159</sup> Additionally, we used the following physics parameterizations: WSM (WRF Single-Moment)

<sup>160</sup> 6-class graupel microphysics scheme (?), Kain-Fritsch cumulus scheme (?), CAM shortwave and

<sup>161</sup> longwave radiation schemes (?). These settings are supported by the one-year test running result

<sup>162</sup> with different options of cumulus scheme and radiation schemes. For the boundary layer, the

<sup>163</sup> Yonsei University scheme (YSU) (?) and the Noah Land Surface Model (?) were used. Both

<sup>164</sup> were chosen as they are common for climate applications that balance long-term reliability and  
<sup>165</sup> computational cost.

<sup>166</sup> *b. Datasets*

<sup>167</sup> For validation purpose, available reanalysis and gridded observational datasets of the highest  
<sup>168</sup> quality are employed (see Table 1). These data products incorporate station measurements or  
<sup>169</sup> satellite information and other data. Although these products are generally based on observations,  
<sup>170</sup> they are based on different network of weather stations. And these datasets are scaled and gridded  
<sup>171</sup> using varied interpolation techniques, elevation model and processing algorithms. In this way,  
<sup>172</sup> using more reference datasets rather than one is important to account for the uncertainties, for  
<sup>173</sup> assessing the performance of the WRF and CESM simulations in terms of both mean behavior and  
<sup>174</sup> variability. We acknowledge that reanalysis products are particularly sensitive to model choice  
<sup>175</sup> and choice of assimilated observations and so cannot be treated as truth. Detailed descriptions of  
<sup>176</sup> these datasets are as follows.

<sup>177</sup> (i) *NARR*: The North American Regional Reanalysis (NARR) (?) provides dynamically down-  
<sup>178</sup> scaled data over North America at  $\sim 32$  km resolution and 3 hourly intervals from 1979 through  
<sup>179</sup> present. All major climatological variables are present in NARR, making it an excellent candidate  
<sup>180</sup> for assessment of regional climate. Nonetheless, some inaccuracies have been identified in NARR  
<sup>181</sup> that must be accounted for, including deficiencies in precipitation fields away from the continental  
<sup>182</sup> US (?).

<sup>183</sup> (ii) *Daymet*: Daymet is an extremely high resolution (1 km) gridded dataset with daily outputs  
<sup>184</sup> of total precipitation, humidity, and minimum/maximum temperature covering the years of 1980  
<sup>185</sup> through 2013 (???). The dataset is produced using an algorithmic technique that ingests point  
<sup>186</sup> station measurements in conjunction with a truncated Gaussian weighting filter. Some adjust-  
<sup>187</sup> ments are made to account for topography. Daymet is available through the Oak Ridge National  
<sup>188</sup> Laboratory Distributed Active Archive Center (ORNL DAAC).

189 (iii) PRISM: The Parameter-elevation Regressions on Independent Slopes Model (PRISM) (?)  
190 supports a 4km gridded dataset obtained by taking point measurements and applying a weighted  
191 regression scheme that accounts for many factors affecting the local climatology. The datasets  
192 include total precipitation and minimum, maximum and (derived) mean temperatures. Monthly  
193 climatological variables are available for 1895 through 2014. Daily data is available for the period  
194 1981 through present, although the documentation is careful to state that since the observational  
195 input changes over time this data is not intended for multi-decadal trends. This dataset will be  
196 used for detection and characterization of temperature and precipitation extremes.

197 (iv) UW: The UW daily gridded meteorological data is obtained from the Surface Water Mod-  
198 eling group at the University of Washington (??). UW incorporated topographic corrections by  
199 forcing the long-term average precipitation to match that of the PRISM dataset. Temperature  
200 dataset is produced in a similar fashion as precipitation, but used a simple 6.1 K/km lapse rate for  
201 topographic effect.

202 *c. Topography*

203 The grid-scale topography for all simulations is contrasted in Figure 3. The higher resolution  
204 simulations provide a much finer representation of regional topography. This is important for  
205 understanding local climate since topography is an important driver for fine-scale dynamic pro-  
206 cesses, especially over complex terrain. Some differences are also apparent between the 28km  
207 varres-CESM and 27km WRF model, particularly over the Central Valley, and indicative of a  
208 different methodology for preparation of the topography dataset.

209 *d. Methodology*

210 We have analyzed both the near surface (2 meter) temperature and precipitation over California,  
211 in order to assess the models' performances in representing the mean climatology. Specifically,  
212 evaluation will focus on daily maximum, minimum and average 2m temperatures (Tmax, Tmin  
213 and Tavg), and daily precipitation (Pr). These variables are key for a baseline climate assessment,  
214 particularly for their relationship with water resources, agriculture and health. With the overall  
215 warm climate and large impact of heat waves over CA, we will focus on the summer season over  
216 June, July and August (JJA) in the aspect of temperature. Since the vast majority of precipitation  
217 in CA occurs in the winter season, together with the accumulation of snowpack, in this way,  
218 precipitation over December-January-February (DJF) will be emphasized. Those seasons also  
219 represent the most part of the climate variability.

220 In order to adequately account for natural variability even regionally, simulations need to be run  
221 long enough. However, there is no particular timeframe for climatology studies. Average weather  
222 conditions over 30-year or so are typically used to track climate to make sure that the data is long  
223 enough to calculate an average that is not influenced by year-to-year variability (?). In this study,  
224 26-year current-climate runtime is chosen to reasonably balance the reproducibility and computa-  
225 tional availability. We have studied the variability of mean temperature and precipitation in both  
226 simulations and observations over 5, 10, 20 and 25 seasons or years, and the results showed that  
227 20 or 25 years' simulation are long enough to adequately capture the regionally climate variability.  
228 30 years or longer run time may sound better, but are not necessary for our case.

229 All the results showed in the following part are based on the time period year 1980 to 2005. All  
230 the datasets have been investigated first to see if time trend exists over this 26 years period, and the  
231 trend has been removed from original datasets if existing. It is found that for temperature, there do

232 exist statistically significant linear trend over some part of CA under the two-tailed level of 0.05.

233 However, no significant trend has been detected for precipitation.

234 Further, in order to better assess the treatment of California's varied climate regions, the state  
235 has been divided into five regional zones, including: the Central Valley, Mountain Region, North  
236 Coast, South Coast, and Desert Region (Figure 1). The division of these five zones are loosely  
237 based on the results of Abatzoglou et als study (?) and the building climates zones from California  
238 Energy Commission. For parts of the results analyses, simulations and datasets are masked to  
239 restrict climate variables to specific zones.

240 Some statistical measurements have been used to quantify the performances of the models com-  
241 paring with the reference datasets. These statistical variables include the Root-mean-square devia-  
242 tion (RMSD), mean absolute difference (MAD), mean relative difference (MRD) and correlation,  
243 and sample standard deviation.

244 When calculating the difference at grid point, the reference datasets are remapped to the given  
245 model's output resolution. Datasets are remapped using a bilinear interpolation method, which  
246 has been verified to provide satisfactory performance. Other remapping algorithms, such as patch-  
247 based have been tested and do not exhibit notable differences.

248 **add more citations in this aspect.**

### 249 **3. Results**

#### 250 *a. Temperature*

251 The mean JJA Tmax, Tmin and Tavg climatology over 26 years are shown in Figure 4. And the  
252 statistical measurements over whole CA area are showed in Table 2. All simulations captured the  
253 spatial climate patterns showed by the PRISM, with high spatial correlations (>0.95), especially

254 for Tmax and Tavg. For Tmax, comparing reference datasets, CESM simulations showed warmer  
255 climate generally, especially uniform CESM. However, WRF output displayed overall colder cli-  
256 mate, especially the WRF 9km. Tmax overall Central Valley has been overestimated by all the  
257 simulations.

258 For Tmin, varres-CESM showed a larger warm effect, with a particularly egregious overestima-  
259 tion of Tmin over Nevada (although difference are much smaller when focusing exclusively on  
260 California). Comparing with reference datasets, WRF had a little smaller difference than varres-  
261 CESM. However, the pattern of Tmin present in Figure 4 in both WRF simulations suggests a  
262 cooler interior to the Central Valley and warmer perimeter, which is not supported by observa-  
263 tions. Overestimation of Tmin by varres-CESM leads a similar overestimation for Tavg. And  
264 underestimation of Tmax by WRF, causes a underestimation for Tavg. The sample standard devi-  
265 ation of the JJA Tmax, Tmin and Tavg by models and PRISM are showed in Figure 5. It can be  
266 seen that the variability has little changes across difference sub-zones, and the values are around  
267 0.5 to 1.5 °Cfor all the datasets, except some higher values over mountains regions in WRF 9km.

268 The RMSD values between the models and reference datasets range from 2 to 4°C. Though un-  
269 certainties, as we already discussed, are showed within reference datasets, it can still be seen that  
270 varres-CESM is comparable to WRF and uniform CESM. Overall, varres-CESM 0.125 degree  
271 performed better in simulating long-term Tmax, WRF is better at modeling Tmin than varres-  
272 CESM. Varres-CESM overestimated all JJA temperatures (especially Tmin), whereas WRF un-  
273 derestimates Tmax and Tavg. When comparing against NARR (not showed), the overestimation  
274 of Tmin are largely reduced for varres-CESM. This suggests that the source of the temperature  
275 bias in varres-CESM and NARR may be related. Also, there are a positive 2 K SST bias near  
276 the California coastline, when comparing varres-CESM and WRF simulations. This may cause  
277 overestimation of temperatures.

278 This is especially encouraging since differences in the varres-CESM simulations, which only  
279 used prescribed SSTs, closely matched those of WRF, which were also forced at the lateral domain  
280 boundaries with reanalysis data. Differences between the reference datasets is relatively smaller  
281 than between the models and reference datasets, thus uncertainties are unlikely impacting the  
282 evaluation results. Also, the sea breeze effect, associated with cooler temperatures near the San  
283 Francisco Bay, are apparent in all runs.

284 The seasonal cycle of Tavg is shown in Figure 7 for simulations and reference data from PRISM  
285 and NARR. The models do show good consistency with reference data with no larger than a 2°C  
286 difference, which mainly occurred in the coldest and hottest seasons. Compared with PRISM,  
287 Varres-CESM showed positive difference over the summer season in all sub-zones except coastal  
288 regions, and negative difference over winter season in all zones. The uniform CESM is similar to  
289 varres-CESM, with larger difference. WRF showed better performance in presenting the monthly  
290 trend than CESM with a little underestimation over all seasons. No notable differences can be  
291 discerned when comparing models across resolutions.

292 The variability over each month is expressed by the sample standard deviation showed in Figure  
293 ???. Generally, local variability of Tavg is under the magnitude of 3°C, mostly within the range  
294 from 1 to 2°C. Among the simulations, WRF 27km is most consistent with PRISM. WRF 9km  
295 is also close to PRISM, but has 1°C larger variability over January and February. Varres-CESM  
296 basically showed more scattered values comparing to reference datasets, and uniform CESM has  
297 a little lower variability than others.

298 For the temperature climatology in California, we are most interested in the Tmax over summer  
299 season due to the impact of summer heat extremes. We depict the frequency distribution of Tmax  
300 using all the JJA daily values over 26 years. The results of the simulations and reference datasets  
301 including Daymet and UW are showed in Figure 8. Properties of the Frequency distribution, in-

302 cluding average, variability, skewness and Kurtosis are tabulated in Table ???. Though with some  
303 deviations, similar distribution shapes with tails off to left are present for both models and obser-  
304 vations. Contrasting with WRF, varres-CESMs are more close to reference datasets. WRF 9km  
305 tended to be colder. Models including varres-CESM and WRF 27km are more consistent with  
306 observations for higher values than the peak and less consistent at lower values. For representa-  
307 tion of heat extremes, both varres-CESM and WRF 27km exhibit satisfactory performance over  
308 most regions except in Central Valley (CV). No obvious improvement is associated with higher  
309 resolution in varres-CESM.

310 In the CV, the models show a clear warm effect and associated long tail, with temperatures  
311 reaching near 50°C. As discussed before, all models do overestimate Tmax in the CV. In order to  
312 further assess the accuracy of the gridded observations, we examine the Tmax data directly from  
313 recorded weather station observations over the CV. The results validate that Tmax values above  
314 45°C are rare (although station observations suggest these days may be slightly more frequent  
315 than suggested by UW and Daymet). The warm bias associated with the aforementioned extreme  
316 hot days in both varres-CESM and WRF is likely due to reasons discussed in ? where biases  
317 were correlated with overly dry summertime soil moisture. This could be caused by the lack  
318 of accurate land surface treatment in climate models. areas. Bonfils and Lobell (2007) found  
319 that irrigation in California's Central Valley has significantly decreased summertime maximum  
320 temperatures especially in heavily-irrigated areas (?). Other studies can also be found for the  
321 cooling climatic effects of irrigation, such as (?).

322 *b. Precipitation*

323 California is known for the shortage of natural water resources with extreme drought over sum-  
324 mer season. Instead, the winter season is particularly important for California as it accounts for 50

percent of the 22.5 inches that California receives for its total annual average precipitation amounts (<http://www.ncdc.noaa.gov/cag/>).

The long-term average climatologies of DJF and annual daily precipitation (Pr) over 26 years from simulations and reference datasets are displayed in Figure ???. And the statistical measurements over whole CA area are showed in Table ???. As we can see, precipitation is distributed mostly along the North coast and Sierra Nevada mountains, and is relatively sparse in other regions. As temperature, simulations also captured the spatial patterns of the PRISM, with high correlation coefficients (>0.94). However, there does exist clear differences among simulations.

Varres-CESM overestimates total precipitation, especially in the coarse resolution (28 km) simulation (about 40%-50%) along the western side of Sierra Nevada. The finer resolution simulation produces a slight reduction of difference with magnitude near 1 mm/day, likely due to improved treatment of orographic effects as showed in Figure 3. Uniform CESM has slighter better results than varres-CESM 0.25deg. Notably, there are large differences between WRF 27km and WRF 9km. WRF 27km underestimates precipitation slightly (about 30%), whereas WRF 9km shows a large positive difference (about 70%-80%) along the North coast and the Sierra Nevada of up to 50 percent. Overall, varres-CESM 0.125° performs slightly better than CESM 0.25° and WRF 27km, as further exhibited by the RMSD values in Table 4. The reference datasets also have notable differences indicating uncertainty inherent in interpolating station data to a grid. However, these observations are still of the highest quality available and the uncertainty is relatively small compared with difference from the simulations.

The climatological annual cycle of precipitation averaged over each sub-region is presented in Figure 11. It can be seen that simulations showed similar trend as reference datasets. The main deviation occurred during the rainy seasons, especially in winter. WRF 27km is drier in all regions and WRF 9km is far wetter in all regions. Varres-CESM tracks well with observed precipitation

349 everywhere except in the Central Valley, where precipitation is overestimated. Nonetheless, the  
350 strong seasonal dependence on precipitation is apparent in all regions with extremely dry condi-  
351 tions during summer months. A slight increase in summertime precipitation is apparent in the  
352 Desert region, indicating the North American monsoon. Overall, varres-CESM is more consis-  
353 tent with observations in most regions and in all seasons compared with WRF. However, we also  
354 observe that the peak month for precipitation tends to occur earlier in varres-CESM than in obser-  
355 vations. It is not surprising that a seasonal time drift occurred with the varres-CESM simulations  
356 as it was not forced by a reanalysis dataset (unlike the WRF simulations).

357 The variability over each month is expressed by the sample standard deviation showed in Figure  
358 ???. It can be seen that variability has similar monthly trend as the annual cycle of precipitation,  
359 with overall value from 0 to 4 mm/day. Varres-CESM also exhibited a slightly larger variability  
360 in the rainy season than observations, while WRF 27km showed a little reduced values. WRF  
361 9km showed notable larger variability compared with observations during rainy seasons over most  
362 regions.

363 The frequency distribution of DJF Pr has been constructed from rainy days in winter  
364 ( $\text{Pr} \geq 0.1 \text{ mm/d}$ ) and depicted in Figure 12. It can be seen that varres-CESM is more consis-  
365 tent with observations everywhere except in the CV. In this region WRF 27km appears to better  
366 capture high-intensity precipitation events, but performs more poorly on low-intensity events. The  
367 underestimation of rainfall frequency in WRF 27km appears consistent across regions. WRF 9km  
368 produces a significantly better treatment of low-intensity events, but greatly overestimates the  
369 frequency of high-intensity events. Notably, varres-CESM 0.25 degree and varres-CESM 0.125  
370 degree do not show significant differences. For strong precipitation events, varres-CESM and  
371 WRF 27km show good performance over most regions except in those noted above, although  
372 these conclusions are also constrained by observational uncertainty.

373 The positive deviation of precipitation using WRF at high resolution has also been found in  
374 former studies. ? also showed that WRF at 12km largely overestimate the precipitation over the  
375 mountain division of CA. The deviation magnitude is less than what showed in this study due to  
376 different division area and different setting of microphysics. In Caldwell's paper aforementioned,  
377 possible reasons have been discussed in detail, stating a variety of source including the model itself  
378 and the choice of physical parameterizations. A comprehensive analysis of the cause of these er-  
379 rors is beyond the scope of this paper. Further discussion can be found in former studies including  
380 the use of different microphysics schemes and resulting change of precipitation magnitude (????).

381 Finally, a concise summary of model performance over CA is provided by the Taylor diagram  
382 (Figure 13). This diagram includes the spatial centered correlation between the simulated and ob-  
383 served fields, the RMS variability of simulations normalized by that in the observations, and mean  
384 differences from reference data. It can be seen that the models correlate well with the PRISM ref-  
385 erence dataset. Normalized standard deviation and bias are larger for precipitation, especially for  
386 WRF 9km. Varres-CESM performed better than WRF generally with essentially an opposite bias  
387 value in many cases. Overall, varres-CESM has demonstrated that it can competitively compare  
388 to WRF in capturing the regional climatology of California.

389 Large-scale features of varres-CESM 0.25° and uniform CESM at 1 degree has been discussed  
390 by Zarzycki et. al. in zarzycki2014multidecadal, zarzycki2015effects and states some important  
391 conclusions of this aspect. It was found that adding refined region over the globe did not affect the  
392 global circulation noticeably. **Colin may want to edit this part.**

#### 393 **4. Discussions and summary**

394 This study has evaluated the performance of the relatively new varres-CESM against dynami-  
395 cally downscaled WRF and gridded reference datasets when simulating California climatology. As

396 the need for assessments of regional climate change is increasing, alternative modeling strategies,  
397 including variable-resolution global climate models will be needed to improve our understanding  
398 of the effects of fine-scale processes in regional climate regulation.

399 Based on 26 years of high-resolution historical climate simulation data over California, we ana-  
400 lyzed both temperature and precipitation in California and across its climate divisions. We found  
401 that varres-CESM output performs slightly better than WRF for mean climatology, although the  
402 model still possessed slight biases towards a warmer and moister climate, especially in the Central  
403 Valley. WRF exhibited a clear cold bias in summer Tmax over most regions except the Central  
404 Valley, but an essentially opposite bias in summer Tmin, especially for the finer resolution simu-  
405 lation. However, looking at the magnitude of RMSD, WRF was better overall at modeling Tmin.  
406 WRF also presented smaller daily temperature variability than both varres-CESM and the observa-  
407 tional datasets. Higher resolution ( $0.125^{\circ}$ ) simulations with varres-CESM were quite similar to the  
408 coarser resolution runs, although there were some improvements in capturing summer maximum  
409 temperature and precipitation. However, WRF 27km shows much better performance than WRF  
410 9km, especially in modeling Tmax and precipitation trends. WRF 27km shows a slightly dryer  
411 climate, but WRF 9km dramatically overestimated precipitation over the North coastal region and  
412 the mountain region. Previous studies have also found this phenomenon for fine-scale simulations  
413 using RCMs as aforementioned. Additionally, we found that almost all of the precipitation comes  
414 from resolved (large-scale) processes for all these models, though convective scheme can also  
415 affect the large-scale microphysics results.

416 Models do show good consistency with reference data for seasonal Tavg, although varres-CESM  
417 exhibited a larger annual range in Tavg with colder winters and warmer summers. The main  
418 precipitation biases occurred during rainy seasons, especially in winter. For describing the extreme  
419 hot events in summer, both varres-CESM and WRF 27km exhibit satisfactory performance over

420 most regions except in Central Valley which may due to overly dry summertime soil moisture.  
421 For strong precipitation events, varres-CESM and WRF 27km show satisfactory modeling ability  
422 over most regions (except the Central Valley, in the case of varres-CESM), although the reference  
423 datasets also show some uncertainties. No obvious improvement is provided by moving from  
424 28km to 14km resolution in varres-CESM.

425 Generally, when compared with observations, simulations do a good job of capturing regional  
426 climatological patterns. Spatial correlations are high between these simulations and observations.  
427 Errors are not indicative of deep underlying problems with the model formulation, but one should  
428 be aware of these biases when using these models for assessing future climate change. Uncertainty  
429 between observational datasets exists, but is much smaller than the models biases. Compared with  
430 the uniform resolution CESM-FV simulation, varres-CESM performed similarly or even better  
431 in some cases. In summary, varres-CESM demonstrated competitive utility for studying high-  
432 resolution regional climatology when compared to a regional climate model (WRF) and a uniform  
433 high-resolution GCM (CESM-FV). This study suggests that variable-resolution GCMs are useful  
434 tools for assessing climate change over the coming century.

435 The importance and necessity of high resolution for regional climate studies has been widely  
436 stressed by previous studies. However, whether the current regional climate models can fulfill  
437 this demand when resolution is pushed to local scales is questionable. Based on our findings,  
438 WRF at 9km grid-scale produced larger biases than at 27km. And further, varres-CESM at 14km  
439 resolution did not demonstrate clear improvement beyond 28km resolution. It is clear that further  
440 work is urgently needed to solve the scale limitation of current regional climate models at fine  
441 horizontal resolutions. The possible causes of the scale limitation may include a lack of accurate  
442 scare-aware physical parameterizations near or below 10 km horizontal resolution, the treatment of

<sup>443</sup> dynamics at fine scales, and the interactions among different components of RCMs or VR-GCMs  
<sup>444</sup> (e.g., land-atmosphere interactions).

<sup>445</sup> *Acknowledgments.* The authors would like to thank Michael Wehner and Daíthí Stone for pro-  
<sup>446</sup> viding the uniform resolution CESM dataset. We would further like to thank Travis O’Brien for  
<sup>447</sup> his many useful conversations on climate model assessment. We also want to thank Xuemeng  
<sup>448</sup> Chen for her assistance in WRF running. This project is supported in part by the University of  
<sup>449</sup> California, Davis and by the Department of Energy “Multiscale Methods for Accurate, Efficient,  
<sup>450</sup> and Scale-Aware Models of the Earth System” program.

## 451 LIST OF TABLES

452	<b>Table 1.</b> Reanalysis and statistically downscaled observational datasets used in this study . . . . .	23
453		
454	<b>Table 2.</b> RMSD, MAD and Correlation (Corr) for JJA temperature over California . . . . .	24
455		
456	<b>Table 3.</b> The first four moments of the JJA Tmax frequency in each sub-zone. Column titles refer to Average (Avg), Variance (Var), Skewness (Skew) and Kurtosis (Kurt). . . . .	25
457		
458	<b>Table 4.</b> RMSD, MAD, MRD, Correlation (Corr) for precipitation over California . . . . .	26
459		
460	<b>Table 5.</b> RMSD, MAD and Correlation (Corr) for MAM temperature over California . . . . .	27
461		
462	<b>Table 6.</b> RMSD, MAD and Correlation (Corr) for SON temperature over California . . . . .	28
463		
464	<b>Table 7.</b> RMSD, MAD and Correlation (Corr) for DJF temperature over California . . . . .	29
465		
466	<b>Table 8.</b> RMSD, MAD, MRD, Correlation (Corr) for precipitation over California . . . . .	30
467		

TABLE 1. Reanalysis and statistically downscaled observational datasets used in this study.

<b>Data source</b>	<b>Variables used</b>	<b>Spatial resolution</b>	<b>Temporal resolution</b>
<b>UW</b>	Pr, T <sub>min</sub> , T <sub>max</sub>	0.125°	daily
<b>PRISM</b>	Pr, T <sub>min</sub> , T <sub>max</sub> , T <sub>avg</sub>	4km	monthly
<b>DAYMET</b>	Pr, T <sub>min</sub> , T <sub>max</sub>	1km	daily
<b>NCEP CPC</b>	Pr	0.125°	daily
<b>NARR</b>	Pr, T <sub>s</sub>	32km	daily, 3-hourly

TABLE 2. RMSD, MAD and Correlation (Corr) for JJA temperature over California

<b>RMSD</b>	<b>UW</b>		<b>PRISM</b>			<b>Daymet</b>	
	$T_{max}$	$T_{min}$	$T_{max}$	$T_{min}$	$T_{avg}$	$T_{max}$	$T_{min}$
<b>varres-CESM 0.25d</b>	2.322	3.745	2.924	3.121	2.604	2.810	3.934
<b>varres-CESM 0.125d</b>	1.900	3.631	2.447	2.944	2.184	2.475	3.701
<b>WRF 27km</b>	2.310	2.738	2.933	2.254	2.169	2.511	2.992
<b>WRF 9km</b>	3.319	2.937	3.492	1.837	1.769	3.203	2.942
<b>uniform CESM 0.25d</b>	3.885	4.088	4.265	3.614	3.536	4.315	4.274

<b>MAD</b>	<b>UW</b>		<b>PRISM</b>			<b>Daymet</b>	
	$T_{max}$	$T_{min}$	$T_{max}$	$T_{min}$	$T_{avg}$	$T_{max}$	$T_{min}$
<b>varres-CESM 0.25d</b>	0.981	2.907	0.606	1.731	0.823	1.177	2.877
<b>varres-CESM 0.125d</b>	0.645	2.848	0.203	1.660	0.579	0.818	2.744
<b>WRF 27km</b>	-0.577	0.819	-0.952	-0.357	-0.771	-0.386	0.789
<b>WRF 9km</b>	-2.277	1.862	-2.720	0.674	-1.142	-2.103	1.757
<b>uniform CESM 0.25d</b>	1.812	2.993	1.449	1.815	1.280	2.013	2.961

<b>Corr</b>	<b>UW</b>		<b>PRISM</b>			<b>Daymet</b>	
	$T_{max}$	$T_{min}$	$T_{max}$	$T_{min}$	$T_{avg}$	$T_{max}$	$T_{min}$
<b>varres-CESM 0.25d</b>	0.998	0.982	0.996	0.986	0.994	0.997	0.979
<b>varres-CESM 0.125d</b>	0.998	0.985	0.997	0.988	0.996	0.997	0.983
<b>WRF 27km</b>	0.997	0.982	0.996	0.989	0.996	0.997	0.978
<b>WRF 9km</b>	0.996	0.985	0.997	0.993	0.998	0.996	0.984
<b>uniform CESM 0.25d</b>	0.994	0.980	0.992	0.981	0.991	0.993	0.977

463 TABLE 3. The first four moments of the JJA Tmax frequency in each sub-zone. Column titles refer to Average  
 464 (Avg), Variance (Var), Skewness (Skew) and Kurtosis (Kurt).

	Central valley				Mountain				North coast				South coast				Desert			
	Avg	Var	Skew	Kurt	Avg	Var	Skew	Kurt	Avg	Var	Skew	Kurt	Avg	Var	Skew	Kurt	Avg	Var	Skew	Kurt
<b>UW</b>	32.6	24.8	-0.8	0.9	26.7	33.2	-0.4	0.3	25.9	30.4	0.1	-0.5	25.9	30.4	0.1	-0.5	37.0	22.9	-0.6	0.7
<b>Daymet</b>	32.7	23.5	-0.9	1.5	25.9	39.3	-0.5	0.5	26.5	30.1	-0.3	0.4	26.5	30.1	-0.3	0.4	37.0	24.3	-0.6	0.6
<b>CESM 0.25d</b>	34.1	26.2	-0.4	0.2	28.1	27.6	-0.4	0.3	26.4	37.4	0.1	-0.7	26.4	37.4	0.1	-0.7	37.6	19.0	-0.5	0.8
<b>CESM 0.125d</b>	34.3	28.5	-0.5	0.4	27.2	30.0	-0.4	0.3	26.3	37.4	0.1	-0.6	26.3	37.4	0.1	-0.6	37.3	21.3	-0.5	0.4
<b>WRF 27km</b>	33.9	34.8	-0.5	0.2	24.9	34.8	-0.3	0.0	26.0	36.7	-0.1	-0.5	26.0	36.7	-0.1	-0.5	36.5	22.6	-0.6	0.5
<b>WRF 9km</b>	32.4	33.1	-0.7	0.6	22.4	38.5	-0.5	0.6	24.9	32.6	0.0	-0.6	24.9	32.6	0.0	-0.6	34.4	24.4	-0.5	0.4

**Notes:** If skew > 0 [skew < 0], the distribution trails off to the right [left]. If kurtosis > 0 [< 0], it is usually more sharply peaked [flatter] than the normal distribution (leptokurtic and platykurtic, respectively).

TABLE 4. RMSD, MAD, MRD, Correlation (Corr) for precipitation over California

Annual	CPC				UW				PRISM				DAYMET				
	RMSD	MAD	MRD	Corr	RMSD	MAD	MRD	Corr	RMSD	MAD	MRD	Corr	RMSD	MAD	MRD	Corr	
<b>varres-CESM 0.25d</b>	0.607	0.394	0.413	0.981	0.616	0.292	0.434	0.968	0.727	0.203	0.429	0.952	0.567	0.191	0.375	0.972	
<b>varres-CESM 0.125d</b>	0.469	0.207	0.321	0.980	0.526	0.115	0.339	0.970	0.624	0.045	0.328	0.961	0.504	0.027	0.310	0.973	
<b>WRF 27km</b>	0.419	-0.205	0.269	0.977	0.580	-0.308	0.274	0.971	0.765	-0.396	0.296	0.965	0.647	-0.409	0.312	0.970	
<b>WRF 9km</b>	2.226	1.485	0.950	0.957	2.052	1.393	0.864	0.964	1.889	1.322	0.815	0.970	2.005	1.306	0.773	0.961	
<b>uniform CESM 0.25d</b>	0.555	0.134	0.277	0.969	0.600	0.031	0.302	0.961	0.700	-0.057	0.290	0.953	0.600	-0.069	0.284	0.962	
DJF		CPC				UW				PRISM				DAYMET			
		RMSD	MAD	MRD	Corr	RMSD	MAD	MRD	Corr	RMSD	MAD	MRD	Corr	RMSD	MAD	MRD	Corr
<b>varres-CESM 0.25d</b>	1.486	0.986	0.532	0.972	1.445	0.673	0.531	0.959	1.654	0.577	0.547	0.943	1.346	0.514	0.435	0.964	
<b>varres-CESM 0.125d</b>	1.194	0.638	0.396	0.976	1.234	0.346	0.398	0.965	1.395	0.287	0.400	0.955	1.170	0.212	0.337	0.969	
<b>WRF 27km</b>	0.888	-0.376	0.269	0.975	1.289	-0.688	0.289	0.967	1.552	-0.785	0.298	0.962	1.351	-0.848	0.324	0.966	
<b>WRF 9km</b>	4.264	2.607	0.742	0.950	3.835	2.315	0.616	0.955	3.570	2.256	0.604	0.964	3.804	2.183	0.554	0.955	
<b>uniform CESM 0.25d</b>	1.392	0.377	0.300	0.960	1.431	0.064	0.316	0.951	1.544	-0.033	0.314	0.946	1.406	-0.095	0.288	0.953	

TABLE 5. RMSD, MAD and Correlation (Corr) for MAM temperature over California

RMSD	UW		PRISM			Daymet	
	T <sub>max</sub>	T <sub>min</sub>	T <sub>max</sub>	T <sub>min</sub>	T <sub>avg</sub>	T <sub>max</sub>	T <sub>min</sub>
<b>varres-CESM 0.25d</b>	1.776	2.212	2.297	2.164	2.033	2.344	2.686
<b>varres-CESM 0.125d</b>	1.727	1.841	2.145	1.883	1.908	2.214	2.287
<b>WRF 27km</b>	1.945	2.062	2.433	1.863	1.991	2.366	2.541
<b>WRF 9km</b>	3.114	2.065	3.060	1.568	1.801	2.969	2.293
<b>uniform CESM 0.25d</b>	2.680	2.112	3.059	2.404	2.674	3.099	2.631

MAD	UW		PRISM			Daymet	
	T <sub>max</sub>	T <sub>min</sub>	T <sub>max</sub>	T <sub>min</sub>	T <sub>avg</sub>	T <sub>max</sub>	T <sub>min</sub>
<b>varres-CESM 0.25d</b>	-0.859	1.308	-0.813	0.681	-0.819	-0.608	1.350
<b>varres-CESM 0.125d</b>	-1.261	0.983	-1.274	0.328	-1.202	-1.052	0.952
<b>WRF 27km</b>	-1.066	0.745	-1.020	0.117	-0.942	-0.818	0.788
<b>WRF 9km</b>	-2.516	1.259	-2.530	0.604	-1.312	-2.305	1.227
<b>uniform CESM 0.25d</b>	-1.191	0.417	-1.139	-0.212	-1.398	-0.938	0.458

Corr	UW		PRISM			Daymet	
	T <sub>max</sub>	T <sub>min</sub>	T <sub>max</sub>	T <sub>min</sub>	T <sub>avg</sub>	T <sub>max</sub>	T <sub>min</sub>
<b>varres-CESM 0.25d</b>	0.997	0.963	0.995	0.963	0.990	0.994	0.942
<b>varres-CESM 0.125d</b>	0.998	0.975	0.996	0.972	0.993	0.995	0.959
<b>WRF 27km</b>	0.996	0.959	0.994	0.968	0.991	0.994	0.937
<b>WRF 9km</b>	0.993	0.971	0.994	0.983	0.994	0.993	0.962
<b>uniform CESM 0.25d</b>	0.993	0.960	0.990	0.949	0.984	0.989	0.938

TABLE 6. RMSD, MAD and Correlation (Corr) for SON temperature over California

RMSD	UW		PRISM			Daymet	
	T <sub>max</sub>	T <sub>min</sub>	T <sub>max</sub>	T <sub>min</sub>	T <sub>avg</sub>	T <sub>max</sub>	T <sub>min</sub>
<b>varres-CESM 0.25d</b>	1.591	3.866	2.065	2.788	1.777	2.088	3.837
<b>varres-CESM 0.125d</b>	1.212	3.906	1.652	2.851	1.524	1.900	3.797
<b>WRF 27km</b>	1.665	3.022	2.111	1.784	1.663	2.059	3.060
<b>WRF 9km</b>	2.262	3.788	2.574	2.322	1.285	2.402	3.615
<b>uniform CESM 0.25d</b>	2.605	3.344	2.970	2.789	2.464	2.999	3.444

MAD	UW		PRISM			Daymet	
	T <sub>max</sub>	T <sub>min</sub>	T <sub>max</sub>	T <sub>min</sub>	T <sub>avg</sub>	T <sub>max</sub>	T <sub>min</sub>
<b>varres-CESM 0.25d</b>	0.122	3.303	-0.353	1.766	-0.240	0.102	3.063
<b>varres-CESM 0.125d</b>	0.394	3.439	-0.126	1.908	-0.048	0.353	3.134
<b>WRF 27km</b>	0.181	2.044	-0.295	0.507	-0.739	0.158	1.807
<b>WRF 9km</b>	-1.412	3.310	-1.931	1.779	-0.673	-1.451	3.004
<b>uniform CESM 0.25d</b>	-0.187	2.415	-0.655	0.877	-0.826	-0.205	2.175

Corr	UW		PRISM			Daymet	
	T <sub>max</sub>	T <sub>min</sub>	T <sub>max</sub>	T <sub>min</sub>	T <sub>avg</sub>	T <sub>max</sub>	T <sub>min</sub>
<b>varres-CESM 0.25d</b>	0.998	0.950	0.996	0.975	0.994	0.996	0.951
<b>varres-CESM 0.125d</b>	0.999	0.957	0.998	0.978	0.996	0.997	0.961
<b>WRF 27km</b>	0.997	0.949	0.996	0.982	0.995	0.996	0.948
<b>WRF 9km</b>	0.996	0.953	0.996	0.986	0.997	0.996	0.959
<b>uniform CESM 0.25d</b>	0.993	0.956	0.992	0.965	0.989	0.991	0.952

TABLE 7. RMSD, MAD and Correlation (Corr) for DJF temperature over California

RMSD	UW		PRISM			Daymet	
	T <sub>max</sub>	T <sub>min</sub>	T <sub>max</sub>	T <sub>min</sub>	T <sub>avg</sub>	T <sub>max</sub>	T <sub>min</sub>
<b>varres-CESM 0.25d</b>	1.959	2.751	2.196	2.015	1.742	2.253	2.700
<b>varres-CESM 0.125d</b>	1.633	2.302	2.035	1.840	1.747	2.089	2.318
<b>WRF 27km</b>	1.699	2.756	2.106	1.734	1.537	2.033	2.665
<b>WRF 9km</b>	1.876	2.753	2.324	1.865	1.324	2.169	2.625
<b>uniform CESM 0.25d</b>	2.979	2.072	3.339	2.500	3.211	3.310	2.408

MAD	UW		PRISM			Daymet	
	T <sub>max</sub>	T <sub>min</sub>	T <sub>max</sub>	T <sub>min</sub>	T <sub>avg</sub>	T <sub>max</sub>	T <sub>min</sub>
<b>varres-CESM 0.25d</b>	-0.549	2.108	-0.984	0.977	-0.920	-0.774	1.836
<b>varres-CESM 0.125d</b>	-0.723	1.678	-1.178	0.541	-1.202	-0.978	1.345
<b>WRF 27km</b>	-0.075	2.027	-0.510	0.895	-0.620	-0.302	1.759
<b>WRF 9km</b>	-1.049	2.214	-1.504	1.077	-0.594	-1.301	1.880
<b>uniform CESM 0.25d</b>	-1.862	-0.010	-2.293	-1.142	-2.616	-2.085	-0.280

Corr	UW		PRISM			Daymet	
	T <sub>max</sub>	T <sub>min</sub>	T <sub>max</sub>	T <sub>min</sub>	T <sub>avg</sub>	T <sub>max</sub>	T <sub>min</sub>
<b>varres-CESM 0.25d</b>	0.989	0.856	0.988	0.925	0.978	0.987	0.856
<b>varres-CESM 0.125d</b>	0.993	0.900	0.991	0.941	0.979	0.989	0.898
<b>WRF 27km</b>	0.992	0.842	0.987	0.931	0.982	0.988	0.838
<b>WRF 9km</b>	0.990	0.859	0.987	0.942	0.987	0.988	0.870
<b>uniform CESM 0.25d</b>	0.980	0.922	0.977	0.885	0.926	0.976	0.893

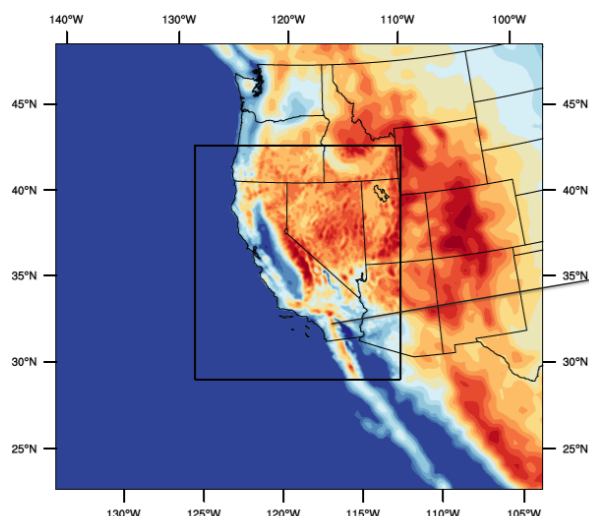
TABLE 8. RMSD, MAD, MRD, Correlation (Corr) for precipitation over California

MAM	CPC				UW				PRISM				DAYMET			
	RMSD	MAD	MRD	Corr	RMSD	MAD	MRD	Corr	RMSD	MAD	MRD	Corr	RMSD	MAD	MRD	Corr
<b>varres-CESM 0.25d</b>	0.542	0.279	0.372	0.981	0.589	0.193	0.412	0.968	0.733	0.083	0.390	0.952	0.553	0.067	0.350	0.971
<b>varres-CESM 0.125d</b>	0.554	0.291	0.371	0.979	0.579	0.217	0.406	0.970	0.678	0.124	0.376	0.958	0.551	0.103	0.348	0.972
<b>WRF 27km</b>	0.448	-0.183	0.267	0.975	0.587	-0.269	0.268	0.970	0.808	-0.378	0.301	0.960	0.675	-0.396	0.309	0.968
<b>WRF 9km</b>	2.143	1.370	0.736	0.966	1.991	1.295	0.667	0.971	1.809	1.203	0.610	0.974	1.924	1.182	0.565	0.967
<b>uniform CESM 0.25d</b>	0.601	0.182	0.295	0.971	0.611	0.096	0.326	0.964	0.725	-0.014	0.308	0.953	0.621	-0.030	0.286	0.963
JJA	CPC				UW				PRISM				DAYMET			
	RMSD	MAD	MRD	Corr	RMSD	MAD	MRD	Corr	RMSD	MAD	MRD	Corr	RMSD	MAD	MRD	Corr
<b>varres-CESM 0.25d</b>	0.138	-0.017	0.347	0.903	0.138	-0.008	0.387	0.905	0.188	-0.038	0.395	0.860	0.147	0.018	0.493	0.885
<b>varres-CESM 0.125d</b>	0.153	-0.006	0.374	0.889	0.148	0.005	0.405	0.897	0.180	-0.022	0.395	0.866	0.167	0.034	0.581	0.866
<b>WRF 27km</b>	0.213	0.010	0.693	0.850	0.186	0.019	0.702	0.892	0.210	-0.011	0.687	0.855	0.202	0.045	0.740	0.879
<b>WRF 9km</b>	1.013	0.644	2.518	0.853	1.000	0.654	2.874	0.881	0.963	0.628	2.511	0.890	1.040	0.684	3.781	0.847
<b>uniform CESM 0.25d</b>	0.177	-0.034	0.471	0.835	0.179	-0.025	0.493	0.837	0.228	-0.055	0.497	0.788	0.198	0.002	0.654	0.780
SON	CPC				UW				PRISM				DAYMET			
	RMSD	MAD	MRD	Corr	RMSD	MAD	MRD	Corr	RMSD	MAD	MRD	Corr	RMSD	MAD	MRD	Corr
<b>varres-CESM 0.25d</b>	0.536	0.346	0.429	0.984	0.579	0.323	0.488	0.966	0.591	0.212	0.443	0.954	0.467	0.188	0.386	0.974
<b>varres-CESM 0.125d</b>	0.381	-0.054	0.309	0.969	0.471	-0.067	0.337	0.956	0.550	-0.165	0.319	0.959	0.494	-0.194	0.342	0.964
<b>WRF 27km</b>	0.382	-0.271	0.288	0.982	0.506	-0.294	0.283	0.971	0.707	-0.405	0.312	0.968	0.618	-0.431	0.337	0.974
<b>WRF 9km</b>	1.851	1.297	1.323	0.960	1.779	1.283	1.339	0.964	1.599	1.185	1.227	0.969	1.671	1.158	1.174	0.962
<b>uniform CESM 0.25d</b>	0.365	0.022	0.331	0.972	0.479	-0.001	0.390	0.955	0.587	-0.112	0.370	0.954	0.491	-0.137	0.366	0.964

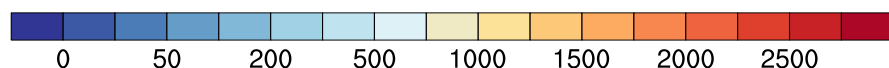
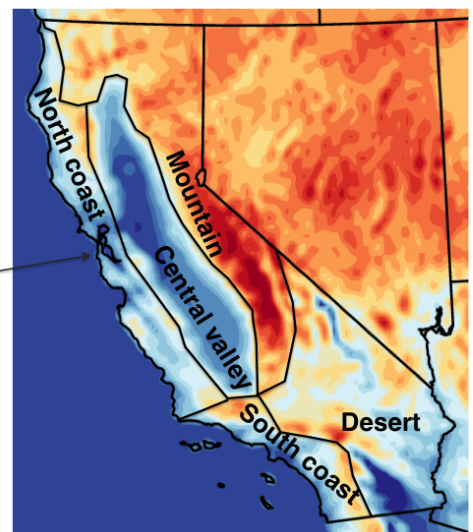
465 **LIST OF FIGURES**

466 <b>Fig. 1.</b>	Domains of WRF simulations (left) and five climate divisions in California (right) with topography in meters (m). . . . .	32
467		
468 <b>Fig. 2.</b>	Approximate regional resolution for the computational grids used in varres-CESM simulations. The dashed lines and solid lines correspond to the outer boundary and inner boundary of the transition region. . . . .	33
469		
470		
471 <b>Fig. 3.</b>	Topography in meters (m) for (top left to bottom right) varres-CESM $0.25^\circ$ , varres-CESM $0.125^\circ$ , uniform CESM-FV $0.25^\circ$ , WRF 27km, WRF 9km and ERA-Interim ( $\sim 80$ km). . . . .	34
472		
473 <b>Fig. 4.</b>	JJA average daily Tmax, Tmin and Tavg from models and reference datasets, and differences between them ( $^\circ\text{C}$ ). . . . .	35
474		
475 <b>Fig. 5.</b>	sample standard deviation of JJA average daily Tmax, Tmin and Tavg from models and PRISM ( $^\circ\text{C}$ ). . . . .	36
476		
477 <b>Fig. 6.</b>	Seasonal cycle of monthly-average Tavg for each subzone ( $^\circ\text{C}$ ). Bars represent standard deviation ( $\sigma$ ) values. . . . .	37
478		
479 <b>Fig. 7.</b>	Seasonal standard deviation ( $s$ ) values of monthly-average Tavg for each subzone ( $^\circ\text{C}$ ). Bars represent standard deviation ( $s$ ) values. . . . .	38
480		
481 <b>Fig. 8.</b>	Frequency distribution of summer Tmax ( $^\circ\text{C}$ ). . . . .	39
482		
483 <b>Fig. 9.</b>	Annual DJF precipitation from models and reference datasets (mm/d). . . . .	40
484		
485 <b>Fig. 10.</b>	As Figure 6, but for monthly-average total precipitation (mm/d). . . . .	41
486		
487 <b>Fig. 11.</b>	As Figure 7, but for monthly-average total precipitation (mm/d). . . . .	42
488		
489 <b>Fig. 12.</b>	Frequency distribution of winter Pr constructed from 26 years of daily data (mm/d) (note that the vertical scale is logarithmic). . . . .	43
490		
491 <b>Fig. 13.</b>	Taylor diagram of annual climatology for the entire California region, using the PRISM dataset as reference. . . . .	44
492		

WRF 9km : Outer and inner domain

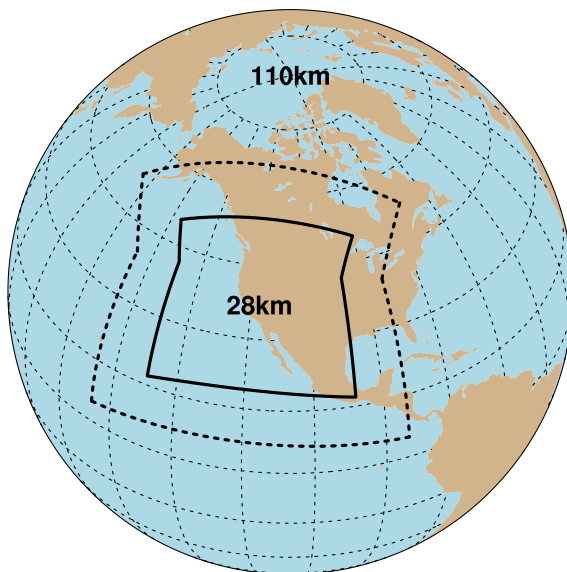


Climate divisions across CA

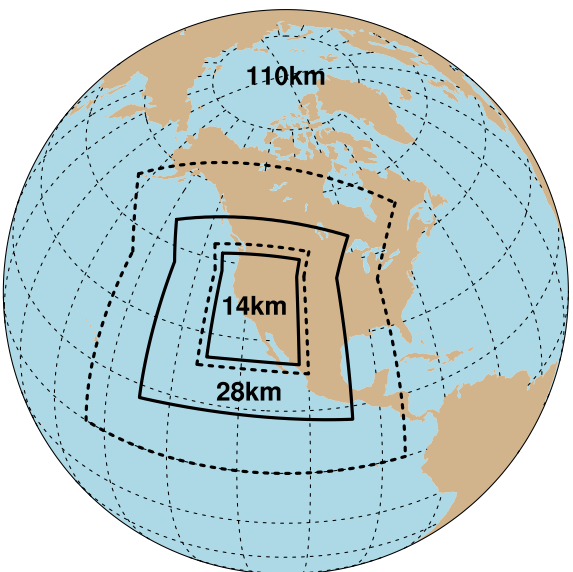


489 FIG. 1. Domains of WRF simulations (left) and five climate divisions in California (right) with topography in  
490 meters (m).

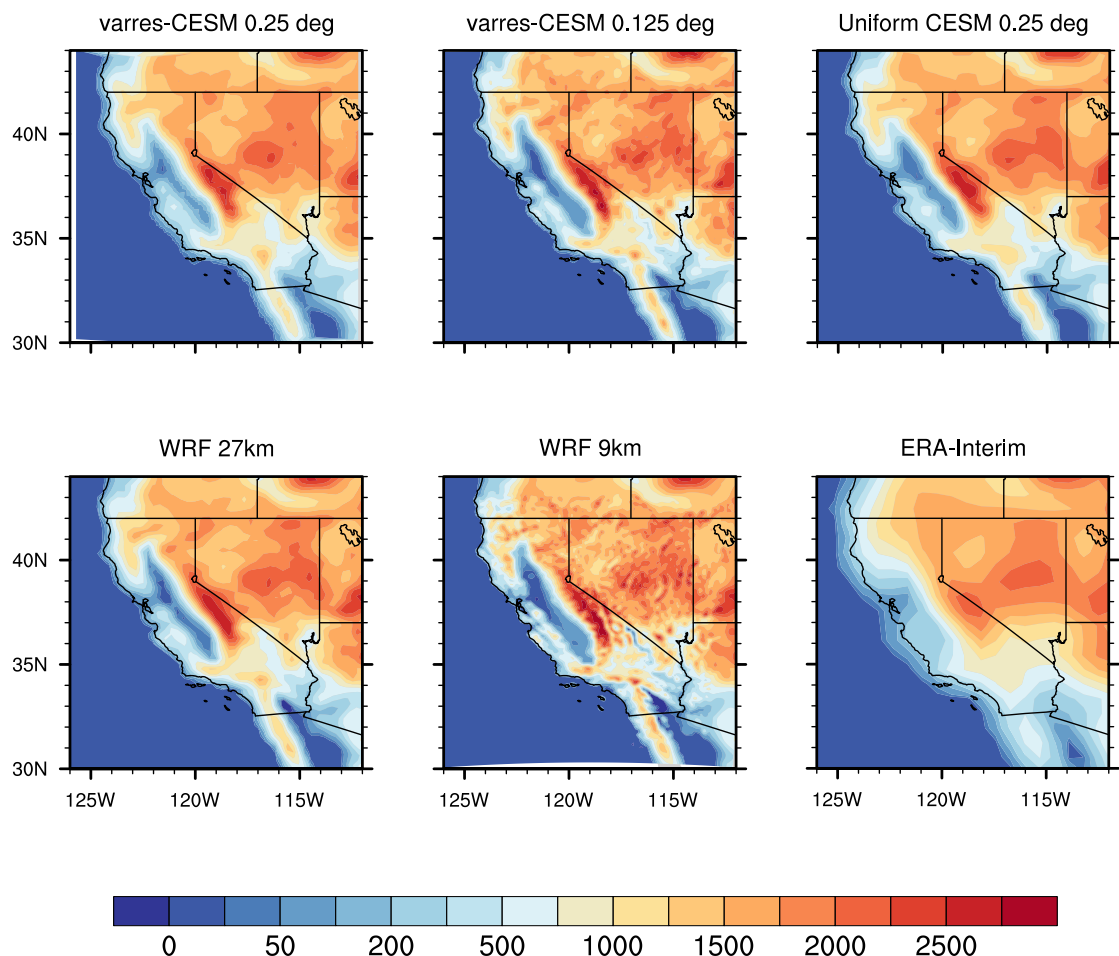
varres-CESM 0.25 degree



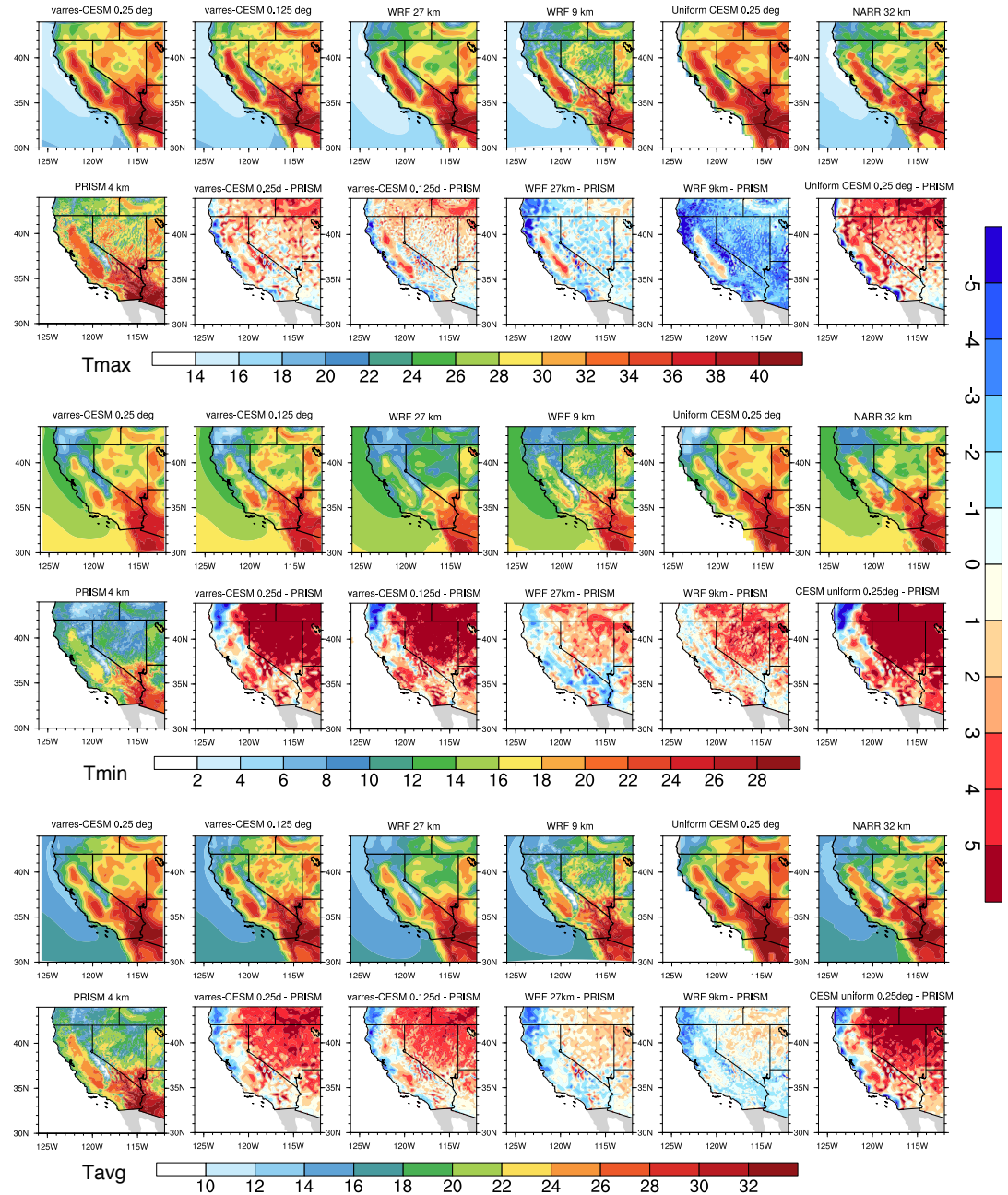
varres-CESM 0.125 degree



491 FIG. 2. Approximate regional resolution for the computational grids used in varres-CESM simulations. The  
492 dashed lines and solid lines correspond to the outer boundary and inner boundary of the transition region.



493 FIG. 3. Topography in meters (m) for (top left to bottom right) varres-CESM  $0.25^\circ$ , varres-CESM  $0.125^\circ$ ,  
 494 uniform CESM-FV  $0.25^\circ$ , WRF 27km, WRF 9km and ERA-Interim ( $\sim 80$  km).



495 FIG. 4. JJA average daily Tmax, Tmin and Tavg from models and reference datasets, and differences between  
 496 them ( $^{\circ}\text{C}$ ).

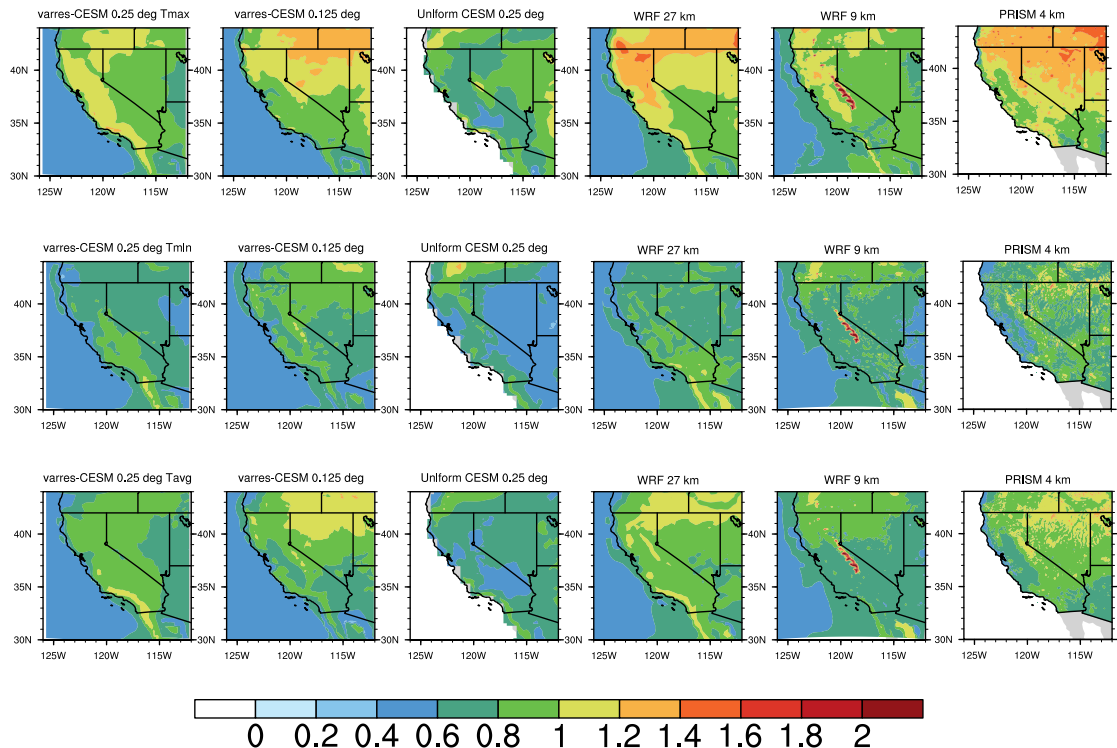
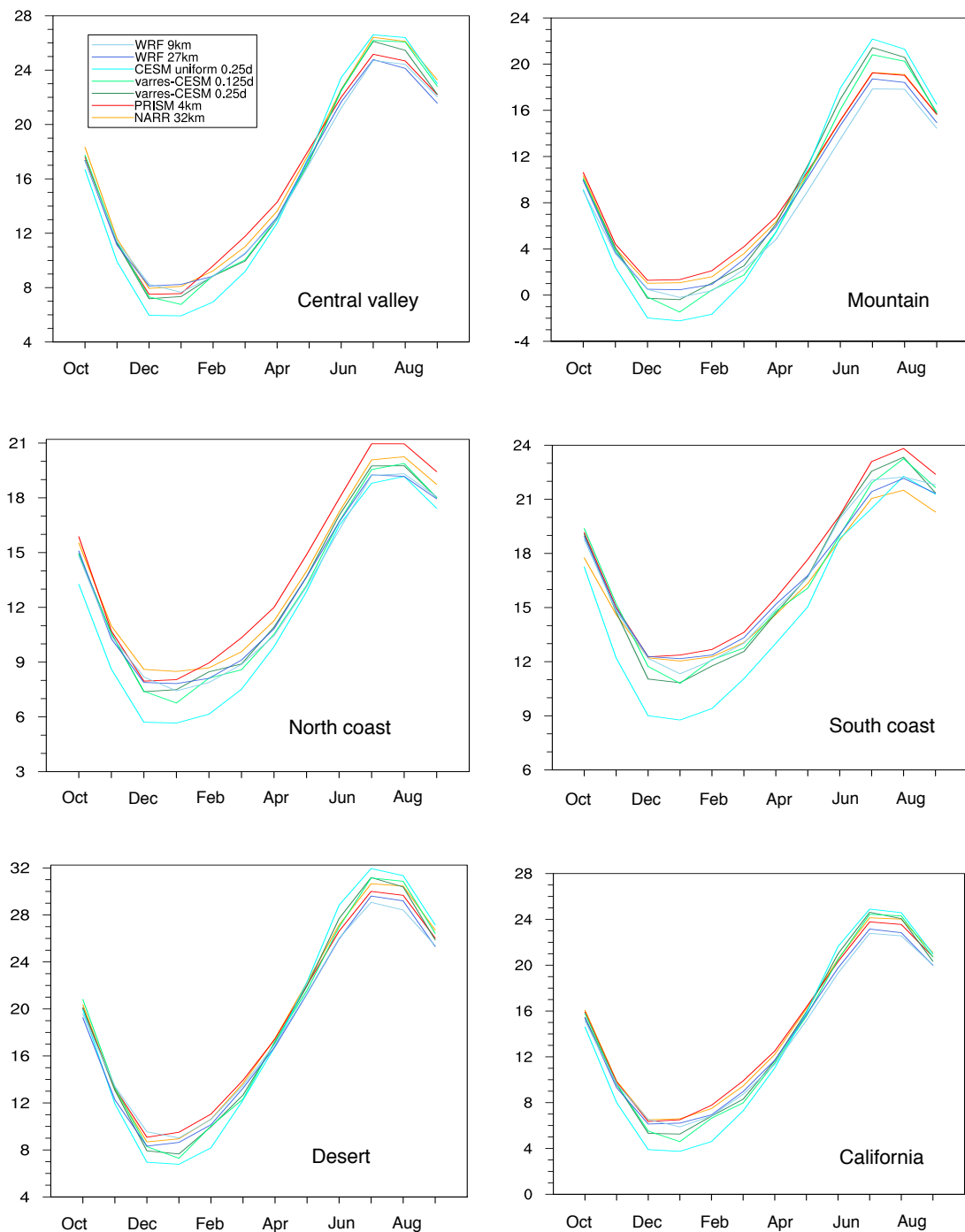
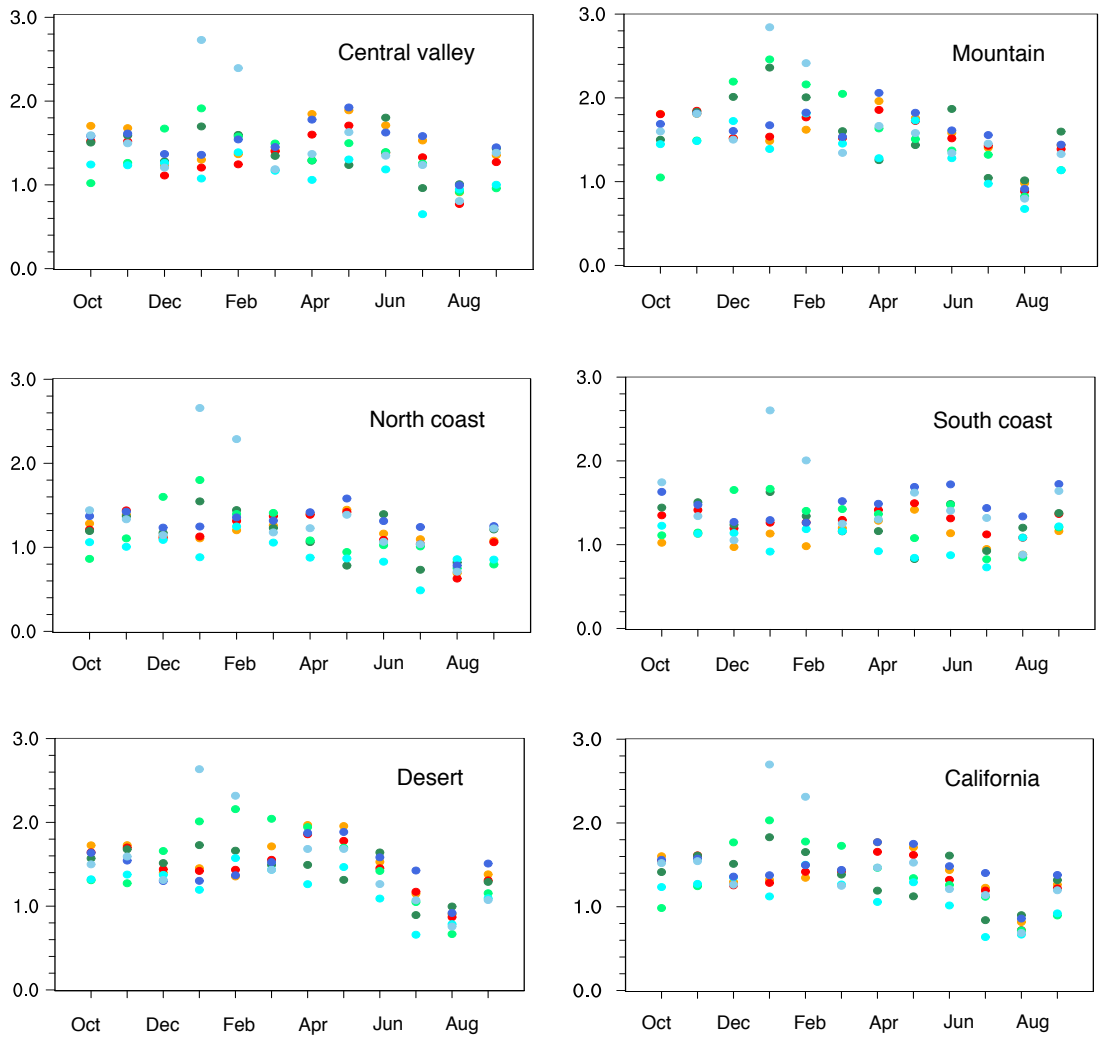


FIG. 5. sample standard deviation of JJA average daily Tmax, Tmin and Tavg from models and PRISM ( $^{\circ}\text{C}$ ).



497 FIG. 6. Seasonal cycle of monthly-average Tavg for each subzone ( $^{\circ}\text{C}$ ). Bars represent standard deviation ( $\sigma$ )  
498 values.



499 FIG. 7. Seasonal standard deviation ( $s$ ) values of monthly-average  $T_{avg}$  for each subzone ( $^{\circ}C$ ). Bars represent  
500 standard deviation ( $s$ ) values.

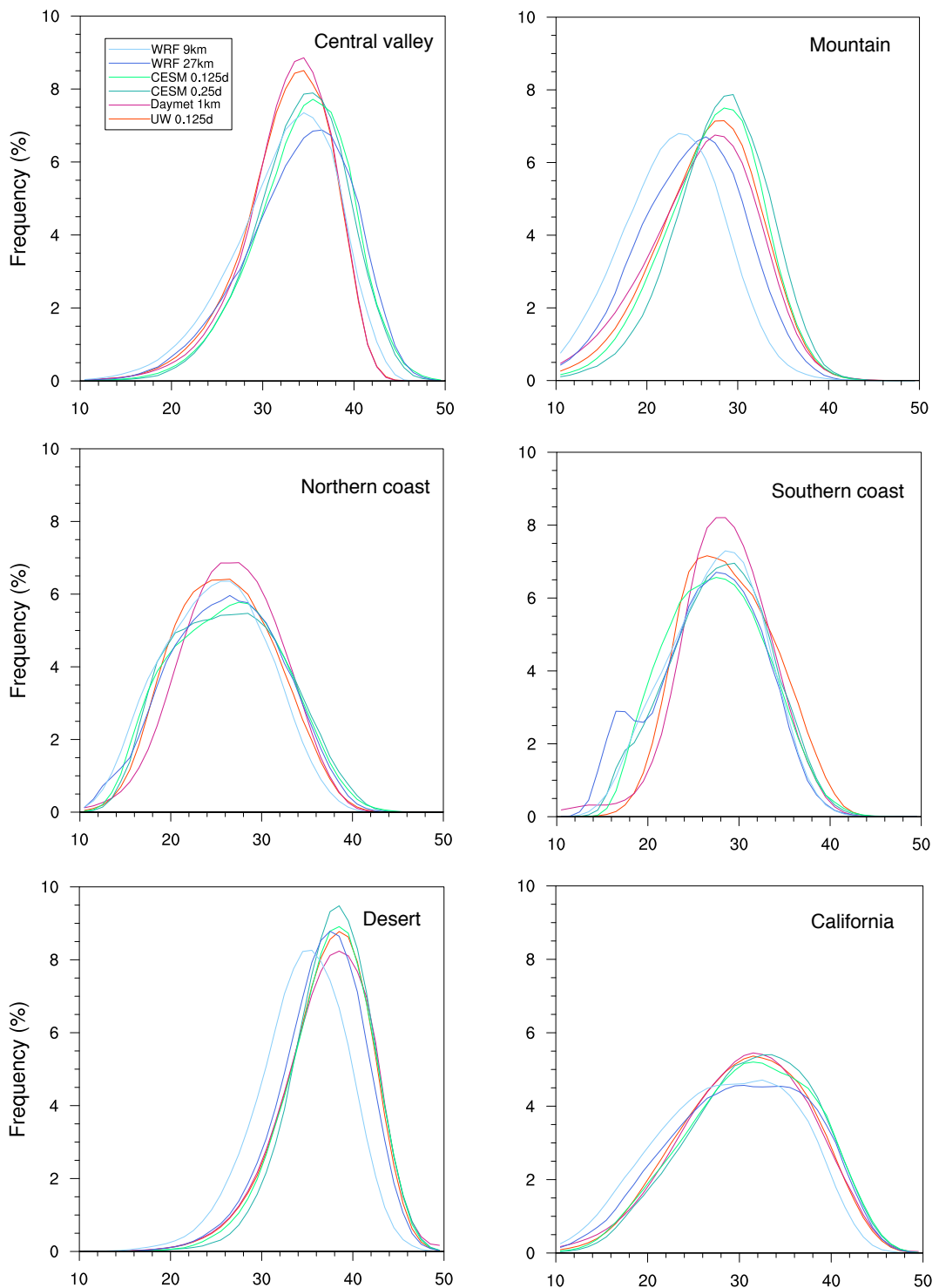


FIG. 8. Frequency distribution of summer Tmax ( $^{\circ}\text{C}$ ).

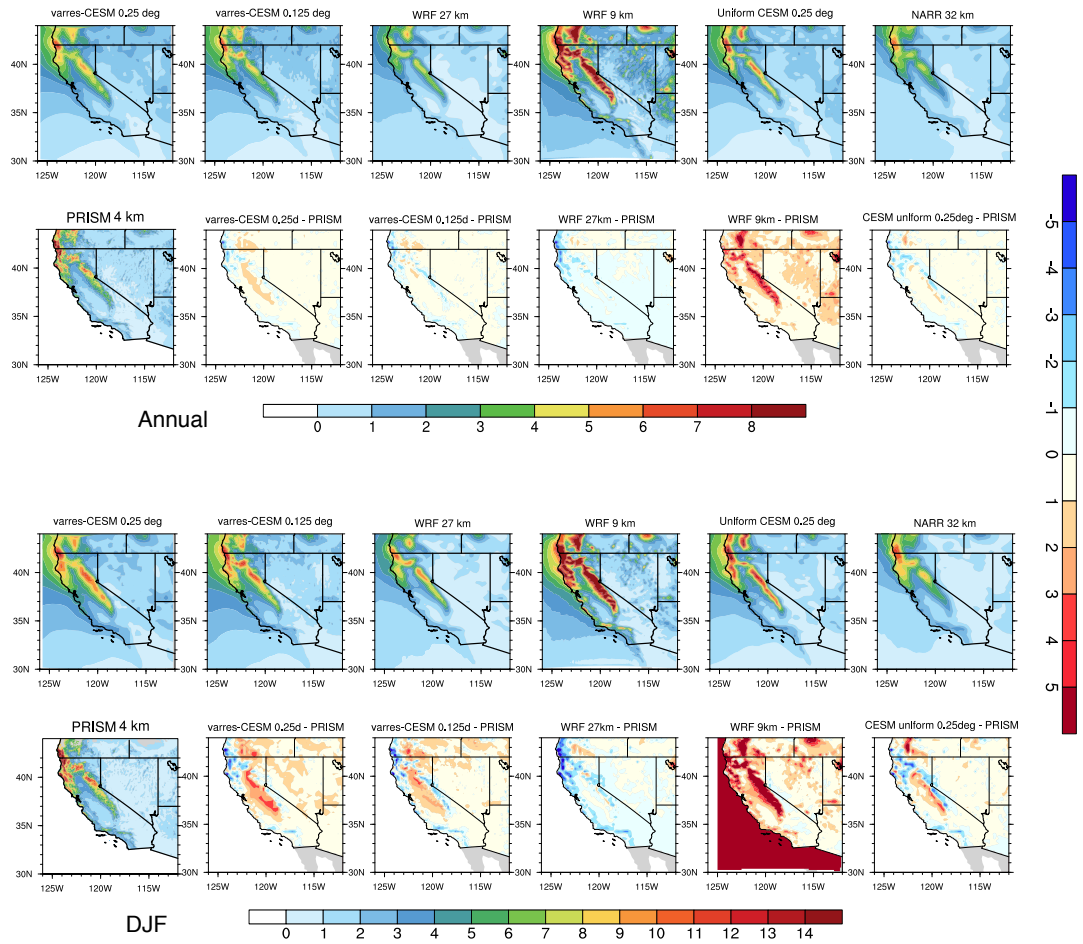


FIG. 9. Annual and DJF precipitation from models and reference datasets (mm/d).

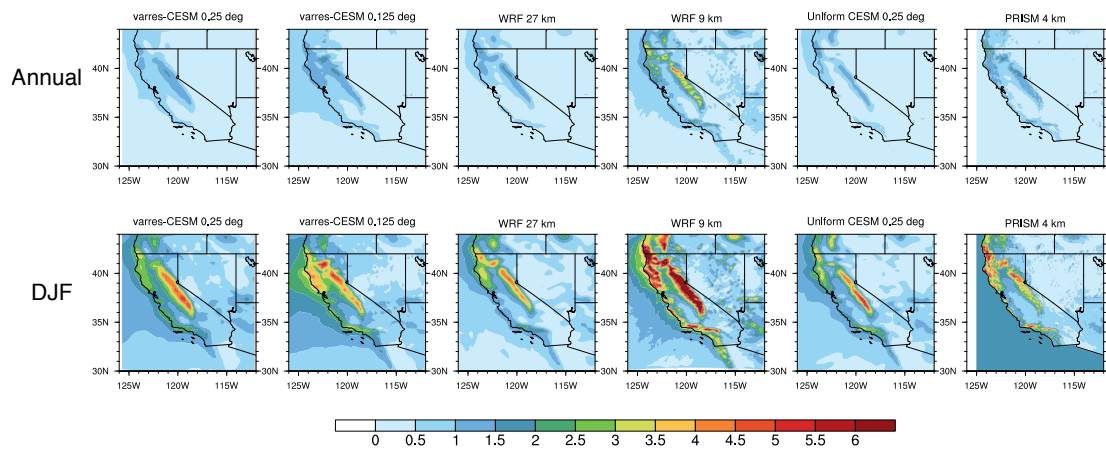


FIG. 10. sample standard deviation of Annual and DJF precipitation from models and PRISM (mm/d).

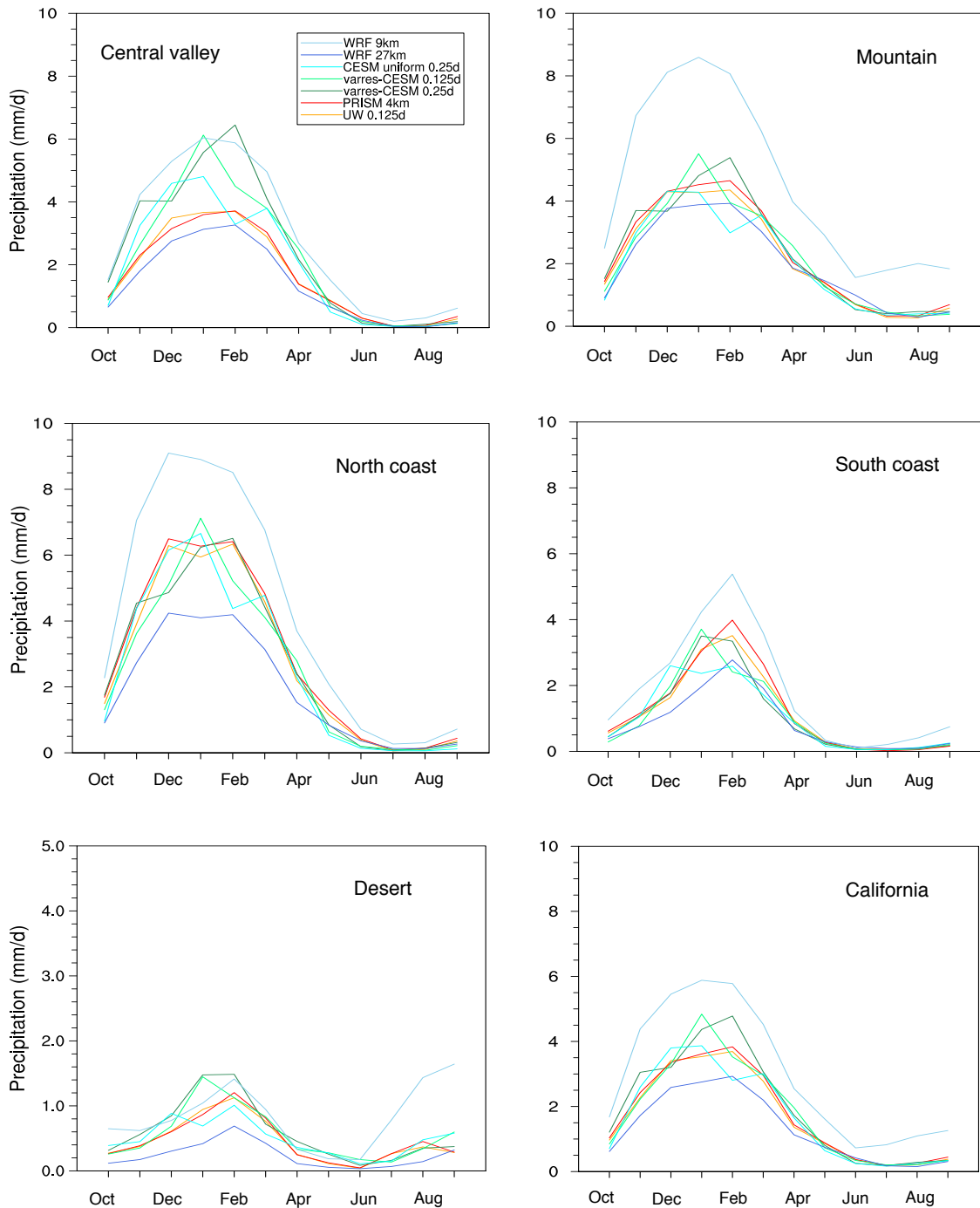


FIG. 11. As Figure 6, but for monthly-average total precipitation (mm/d).

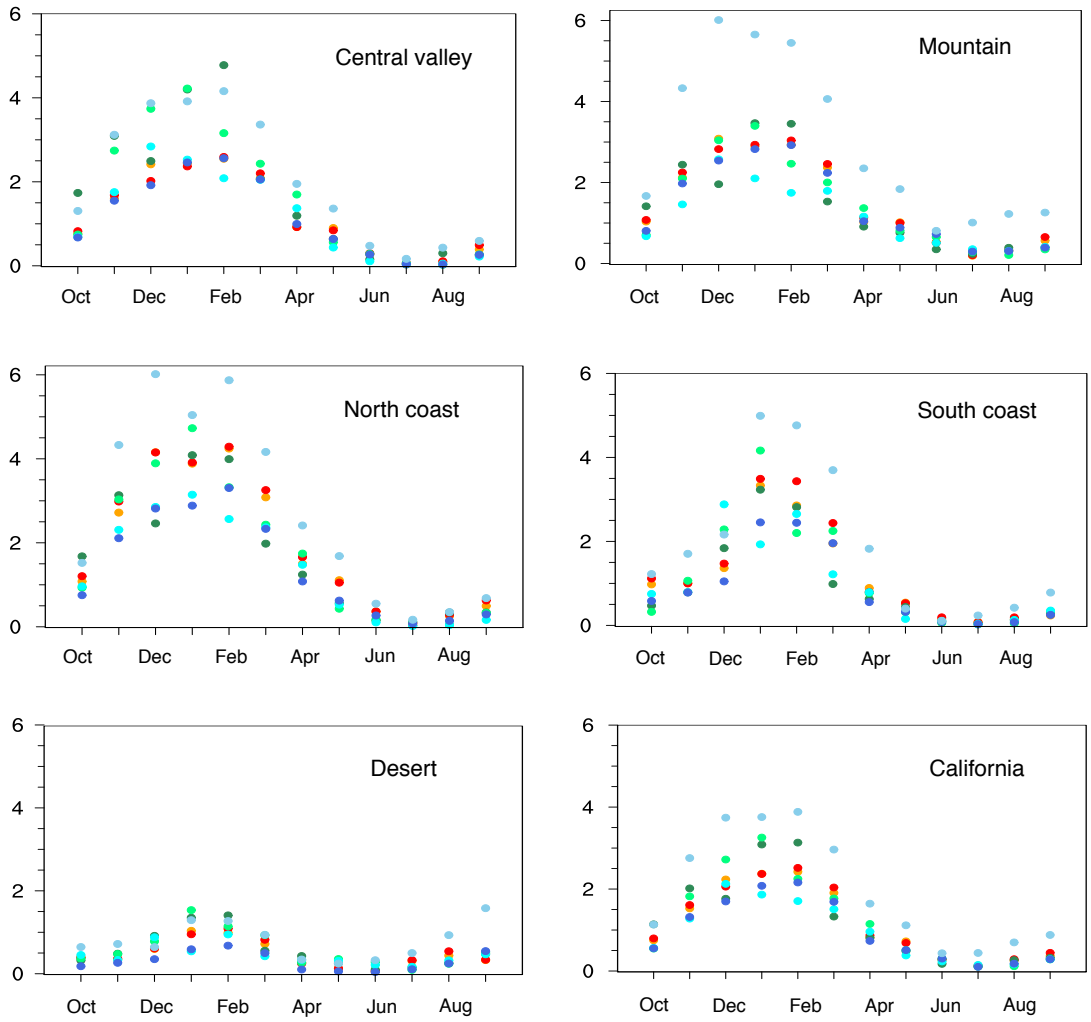
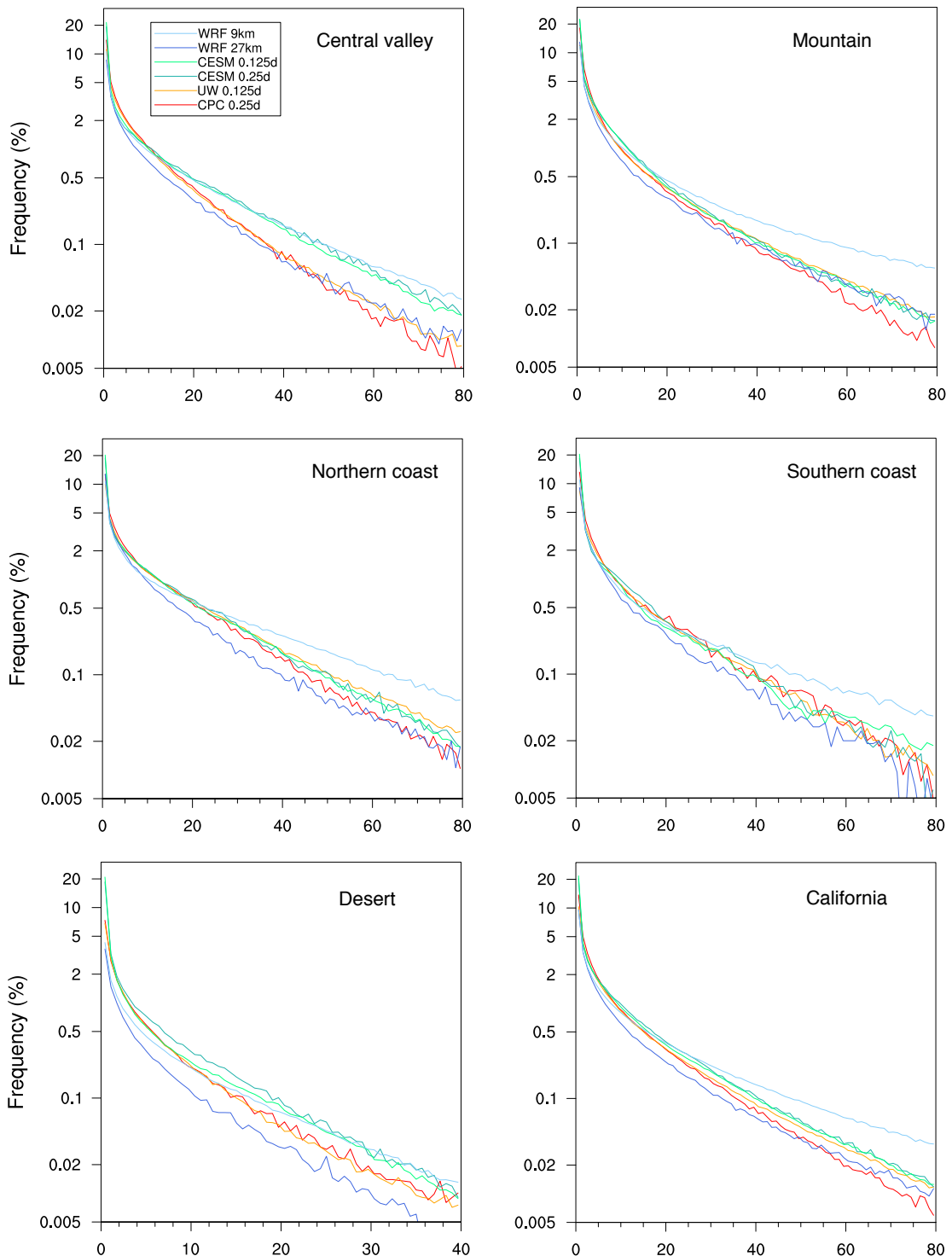
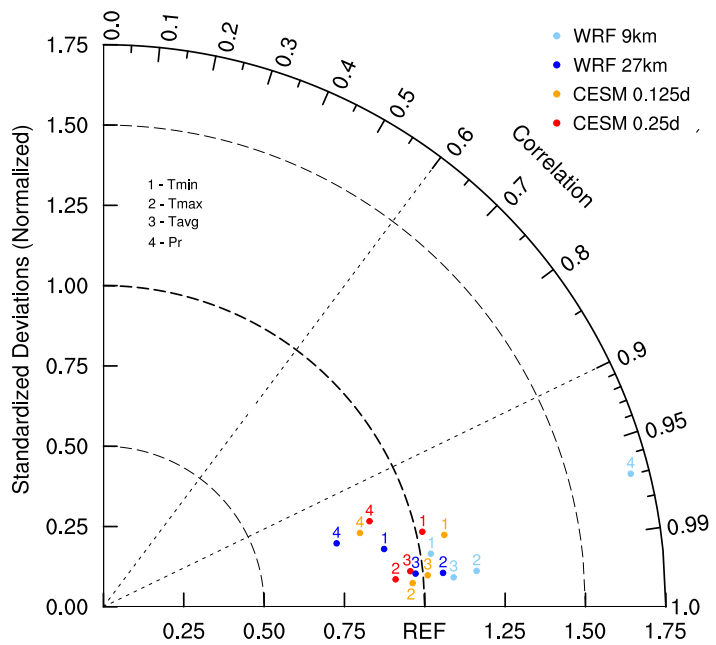


FIG. 12. As Figure 7, but for monthly-average total precipitation (mm/d).



501 FIG. 13. Frequency distribution of winter Pr constructed from 26 years of daily data (mm/d) (note that the  
 502 vertical scale is logarithmic).



503 FIG. 14. Taylor diagram of annual climatology for the entire California region, using the PRISM dataset as  
 504 reference.